Cytochrome *c* polymerization by successive domain swapping at the C-terminal helix

Shun Hirota[a,1], Yoko Hattori[a], Satoshi Nagao[a], Midori Taketa[b], Hirofumi Komori[b,c], Hironari Kamikubo[a], Zhonghua Wang[a,d], Isao Takahashi[a], Shigeru Negi[e], Yukio Sugiura[e], Mikio Kataoka[a], and Yoshiki Higuchi[b,c]

[a]Graduate School of Materials Science, Nara Institute of Science and Technology, 8916-5 Takayama, Ikoma, Nara 630-0192, Japan; [b]Department of Life Science, Graduate School of Life Science, University of Hyogo, 3-2-1 Koto, Kamigori-cho, Ako-gun, Hyogo 678-1297, Japan; [c]RIKEN SPring-8 Center, 1-1-1 Koto, Mikazuki-cho, Sayo-gun, Hyogo 679-5248, Japan; [d]College of Chemistry and Chemical Engineering, China West Normal University, Nanchong 637002, China; and [e]Faculty of Pharmaceutical Sciences, Doshisha Women's University, Koudo, Kyotanabe-shi, Kyoto 610-0395, Japan

Edited* by Chikashi Toyoshima, University of Tokyo, Tokyo, Japan, and approved June 8, 2010 (received for review February 15, 2010)

Cytochrome *c* (cyt *c*) is a stable protein that functions in a monomeric state as an electron donor for cytochrome *c* oxidase. It is also released to the cytosol when permeabilization of the mitochondrial outer membrane occurs at the early stage of apoptosis. For nearly half a century, it has been known that cyt *c* forms polymers, but the polymerization mechanism remains unknown. We found that cyt *c* forms polymers by successive domain swapping, where the C-terminal helix is displaced from its original position in the monomer and Met-heme coordination is perturbed significantly. In the crystal structures of dimeric and trimeric cyt *c*, the C-terminal helices are replaced by the corresponding domain of other cyt *c* molecules and Met80 is dissociated from the heme. The solution structures of dimeric, trimeric, and tetrameric cyt *c* were linear based on small-angle X-ray scattering measurements, where the trimeric linear structure shifted toward the cyclic structure by addition of PEG and $(NH_4)_2HPO_4$. The absorption and CD spectra of high-order oligomers (~40 mer) were similar to those of dimeric and trimeric cyt *c* but different from those of monomeric cyt *c*. For dimeric, trimeric, and tetrameric cyt *c*, the ΔH of the oligomer dissociation to monomers was estimated to be about −20 kcal/mol per protomer unit, where Met-heme coordination appears to contribute largely to ΔH. The present results suggest that cyt *c* polymerization occurs by successive domain swapping, which may be a common mechanism of protein polymerization.

dimer | trimer | protein polymer

Cytochrome *c* (cyt *c*) is a well-known globular heme protein, which transfers electrons from cytochrome bc_1 complex to cytochrome *c* oxidase in the respiratory chain in mitochondria. It also plays a key role in apoptosis, where it is released to the cytosol when permeabilization of the mitochondrial outer membrane occurs (1, 2). Cyt *c* contains three long α-helices (3–5). The heme of cyt *c* forms covalent bonds with two cysteine residues through their sulfur atoms and is coordinated in the native form by His18 and Met80 (3–5). Met80 dissociation induces peroxidase activity and leads to the oxidation of cardiolipin, in turn, leading to the release of proapoptotic factors (6). When heated at 75 °C for 12 h (7, 8), cyt *c* forms amyloid fibrils that are observed in other proteins including those related to neurodegenerative diseases (9). Due to this connection to neurodegenerative diseases, the mechanism of the protein structural change has been studied intensively (10, 11), and oligomeric proteins have gained interest as initial intermediates (12, 13). Recently, the crystal structure of a stable dimer of serpin, a family of proteins that forms large stable multimers leading to intracellular accretion and disease, revealed a domain-swapped structure of two long antiparallel β-strands inserting into the center of the neighboring monomer (14).

Interconversion of monomers and polymers in cyt *c* has been known for nearly half a century (15), but the mechanism of its polymerization is still unknown due to a lack of information on the structural and thermodynamic characteristics of the oligomerization process. By solving the crystal structures of dimeric and trimeric cyt *c* and the solution structures of dimeric, trimeric, and tetrameric horse cyt *c*, we show that cyt *c* molecules form polymers by swapping the C-terminal domain successively.

Results

Ferric horse cyt *c* oligomers were prepared by treatment of monomeric ferric horse cyt *c* with ethanol. The generated dimeric, trimeric, and tetrameric cyt *c* proteins were separated by gel chromatography (Fig. S1). The estimated mass of each purified oligomeric cyt *c* was in agreement with its expected mass. Purified cyt *c* oligomers were stable at 4 °C, although they converted to monomers when heated at 70 °C for 5 min. It is noteworthy that RNase A oligomers dissociate to monomers under similar conditions (heating at 65 °C for 10 min) (16). Production of dimeric cyt *c* from monomeric cyt *c* was detected by adding 4 mM SDS, but a poor yield of larger oligomers was obtained (Fig. S1, curve *F*). Monomeric cyt *c* was also formed from dimeric cyt *c* by SDS addition (Fig. S1, curve *G*). These results indicate the existence of an equilibrium between monomeric and dimeric cyt *c* in the presence of SDS.

The Soret band at 409 nm of monomeric ferric cyt *c* blue shifted to 406.5 nm with increased intensity in the dimer, trimer, and tetramer as reported for the cyt *c* dimer (Fig. S2*A*) (17). The optical absorption spectrum of the species obtained after the trimer was heated at 70 °C for 5 min became similar to that of the purified monomer. The intensity of the 695-nm band characteristic for the Met-heme iron coordination decreased significantly with a red shift of ~5 nm in the absorption spectra of dimeric, trimeric, and oligomeric cyt *c* (Fig. S2*B*). The 695-nm band increased its intensity in the absorption spectrum of the species obtained after the trimer was heated at 70 °C for 5 min. However, there was no significant change among the absorption spectra of oligomers studied. The absorption spectra of oligomeric cyt *c* exhibited the Soret maximum at 406.5 nm and another absorption band at ~529 nm with a shoulder peak at ~562 nm. These properties resemble those of the spectrum of the hydroxide-bound form of Met-depleted cyt *c* (18, 19), which suggests coordination of a hydroxide ion instead of Met in the oligomers, although the presence of the 695-nm band in the oligomers indicates that Met-heme coordination persists in some proportion of the protein. The intensity of the negative 208-nm CD band of the oligomers

Author contributions: S.H. designed research; Y. Hattori, S. Nagao, M.T., H. Komori, H. Kamikubo, Z.W., and I.T. performed research; S.H., Y. Hattori, S. Nagao, M.T., H. Komori, H. Kamikubo, Z.W., S. Negi, Y.S., M.K., and Y. Higuchi analyzed data; and S.H. wrote the paper.

The authors declare no conflict of interest.

*This Direct Submission article had a prearranged editor.

Data deposition: The coordinates for the dimeric and trimeric cyt *c* have been deposited in the Protein Data Bank, www.pdb.org (PDB ID codes 3NBS and 3NBT, respectively).

[1]To whom correspondence should be addressed. E-mail: hirota@ms.naist.jp.

This article contains supporting information online at www.pnas.org/lookup/suppl/doi:10.1073/pnas.1001839107/-/DCSupplemental.

is greater than that of the monomer (Fig. S2*C*). These results indicate that the secondary structure of oligomeric cyt *c* was perturbed. The absorption and CD spectra of larger oligomers with sizes of 30–50 mers were also similar to those of the dimer and trimer. The absorption and CD results suggest that Met80-heme coordination was perturbed significantly in the oligomers and that the original Met80-heme coordination was recovered by heating the oligomeric proteins at 70 °C for 5 min.

To elucidate the detailed structures of cyt *c* oligomers, we have solved the X-ray crystal structures of dimeric and trimeric cyt *c* (Fig. 1). Both structures exhibit domain-swapped structures, where the C-terminal regions beyond Thr78 of the dimer and Lys79 of the trimer are relocated from the original position observed in the monomer due to Met80 dissociation from the heme. The relocated C-terminal region includes one α-helix, and the produced vacant area is occupied by the corresponding region of another cyt *c* molecule. PEG molecules, added for crystallization, were identified in the crystal structures (Figs. S3 and S4). Diethylene glycol lies at the interface between two protomers in dimeric cyt *c*, whereas it interacts with the hinge loop (Thr79–Ala83) in trimeric cyt *c*. These interactions contribute to the stabilization of the dimer and trimer structures, resulting in closed-ended mutual swapping and cyclic structures, respectively. Tetraethylene glycol interacts with Lys55 and sits at the interface between the oligomers in both crystal structures of dimeric and trimeric cyt *c*. This interaction reduces the positive charge of the protein surface and the repulsion between the oligomers in the crystals. However, the linker loop is not long enough to cause domain swapping without steric hindrance and, consequently, perturbation in the protein structure around the heme is induced. The heme-heme distance is shorter in the dimer (18.4 Å) than in the trimer (19.8–20.0 Å). As a result, the Thr78 residual position moves toward the solvent in the dimer, whereas in the trimer it remains in the same position as in the monomer.

There are four independent cyt *c* molecules (two dimers) in the unit cell of the dimeric cyt *c* crystal and six cyt *c* molecules (two trimers) in the unit cell of the trimeric cyt *c* crystal. We have calculated the rmsd of the C-terminal helical region and the rest of the protein (excluding the hinge loop) between the structures of the monomer and each independent protomer of the dimer and trimer (Table S1). The rmsd values of both the C-terminal region and the rest of the protein were less than 0.50. These results indicate that the structures of the C-terminal region are similar between the monomer and the protomers of the dimer and trimer, as well as the rest of the protein excluding the hinge loop. There are six key hydrogen bonds (<3.0 Å between heavy atoms) between the C-terminal region and the other regions of the protein in the monomer (Lys79/Thr47, Phe82/Lys72, Ile85/Leu68, Arg91/Met65, Lys99/Glu61, and Thr102/Gly34) (PDB ID code 1HRC) (Fig. S5). However, there is no hydrogen bond between the C- and N-terminal regions in the monomer, although they are positioned next to each other. The N- and C-terminal helices interact mainly by hydrophobic interaction, and the atoms in these regions exhibit larger temperature factors than those in the rest of the protein molecule. We added ethanol for oligomerization. Alcohol has been demonstrated to stabilize

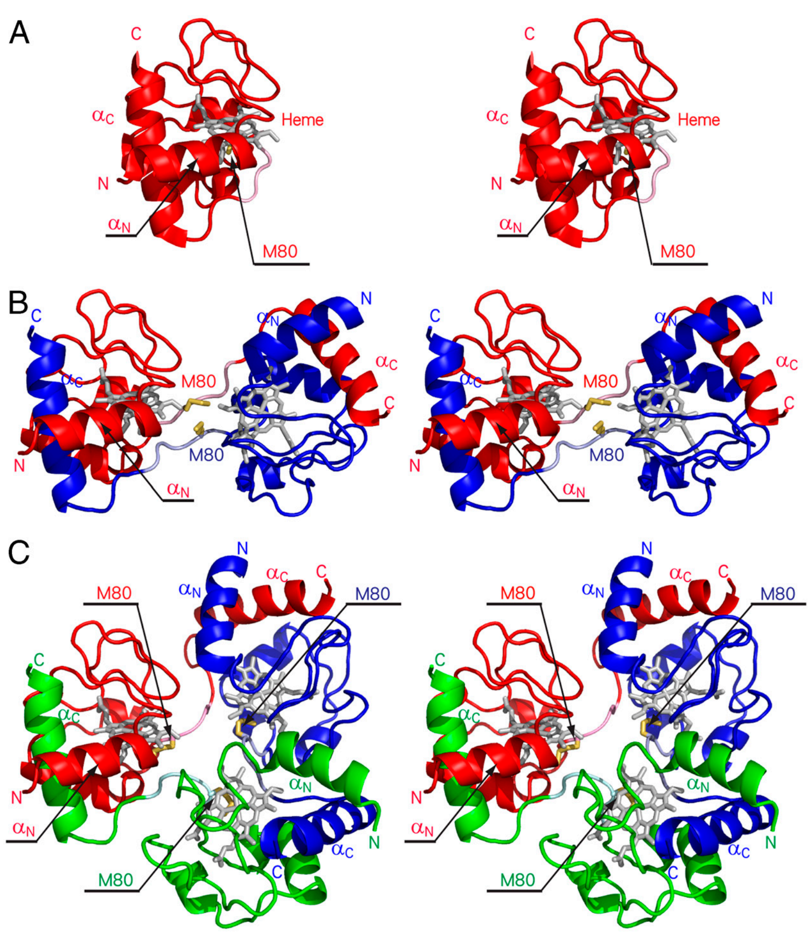

Fig. 1. Schematic representations of crystal structures of oxidized monomeric and oligomeric cyt *c*. (*A*) Structure of monomeric cyt *c* (PDB ID code 1HRC). (*B*) Structure of dimeric cyt *c* (red and blue). (*C*) Structure of trimeric cyt *c* (red, blue, and green). The hemes are shown as gray stick models. Side-chain atoms of Met80 (labeled as M80) are shown as yellow stick models. The N and C termini and the N- and C-terminal helices are labeled as N, C, αN, and αC, respectively. The Thr79-Ala83 residues (hinge loop of the monomer) are depicted in pale colors.

the helical structure in proteins (20). Therefore, the C-terminal region presumably forms a relatively stable helix and maintains its structure during the domain-swapping process due to the addition of ethanol. These properties are presumed to be important for dissociation of the C-terminal region from the rest of the protein and to form successive domain swapping in cyt *c*.

Met80 was dissociated from the heme in cyt *c* oligomers allowing the C-terminal α-helix to swap (Fig. 2). This suggests that Met-heme coordination stabilizes the interaction of the C-terminal helical region with the N-terminal region, resulting in the native monomeric structure. Actually, residues 83–86 are reported to be among the highest disordered regions in the solution structure of horse ferric cyt *c* according to NMR investigations (4). The side chain of Met80 is exposed to the solvent and Phe82 occupies the Met80 position in the dimer, while the side chains of Met80 and Phe82 in the trimer move but stay in the vicinity of their corresponding positions in the monomer. The dissociation of Met80 from the heme iron allows a water molecule or a hydroxide ion to bind in its place. According to the absorption spectra of the dimer and trimer and the previous reports on Met-depleted cyt *c* (18, 19), a hydroxide ion appears to be coordinated to the heme in the crystal (pH 8.5). This hydroxide ion is hydrogen-bonded to Tyr67 in the heme pocket. Recently, it has been shown that the hydrogen bond network around Tyr67 of cyt *c* is associated with the conformational transition of cyt *c* (21). Although the heme pocket environments are different in the dimer and trimer, the similarity in their absorption spectra is due to coordination of the hydroxide ion in both of the oligomers. The peroxidase activity of cyt *c* is thought to play an important role in apoptosis (6), where the activity depends on the perturbation of the Met-heme coordination (22). Actually, the peroxidase activity of dimeric cyt *c* was higher than that of monomeric cyt *c* (Fig. S6).

Surface envelope models of the oligomers were obtained by using small-angle X-ray scattering (SAXS) data to elucidate the structures of the oligomers in solution (Fig. 3). Even though the resolution of the models is about 30 Å, the monomer unit can be resolved in these models. Interestingly, trimeric and tetrameric cyt *c* showed linear structures where the N- and C-terminal monomer units were distant from each other, although the crystal structure of trimeric cyt *c* exhibited a cyclic form. To investigate the effect of precipitants on the trimeric cyt *c* structure, SAXS data were also measured in the presence of PEG 200 and $(NH_4)_2HPO_4$. Although the profile under crystallization conditions was not fully superimposed on the calculated profile, the profile of the trimer shifted from the linear profile toward the estimated profile of the cyclic crystal structure upon addition of PEG 200 and $(NH_4)_2HPO_4$ (Fig. S7*A*). Such a profile change was not observed by adding only 30% PEG or 200 mM $(NH_4)_2HPO_4$ (Fig. S7*B*), whereas cyclic cyt *c* was converted back to a linear structure by removal of both 30% PEG and 200 mM $(NH_4)_2HPO_4$ within the time frame of the experimental process (30 min). These results show that the oligomers are essentially linear in solution but can form cyclic structures by addition of PEG molecules and 200 mM $(NH_4)_2HPO_4$. It can be assumed that the equilibrium between the open-ended linear and closed-ended cyclic forms of trimeric cyt *c* shifts sufficiently toward the cyclic form upon addition of both precipitants.

The results of differential scanning calorimetry (DSC) measurements for purified oxidized oligomeric cyt *c* are shown in Fig. 4. The peak area represents the enthalpy change (ΔH) during the dissociation of the oligomer to the corresponding monomers, whereas the peak temperature (T_m) represents the dissociation temperature. The enthalpy changes during oligomer dissociation are negative, indicating that dissociations of oligomers to monomers are exothermic processes. The enthalpy changes increased for larger oligomers, where ΔH values of the dimer-to-monomer, trimer-to-monomer, and tetramer-to-monomer dissociations were -40 ± 2, -60 ± 4, and -79 ± 3 kcal/mol, respectively. ΔH was decreased by about 20 kcal/mol by elongation of one monomer unit.

No signal was observed in subsequent scanning after reaching 70 °C, which is in agreement with the nonreversible conversion of dimeric and trimeric cyt *c* to monomers by heating. T_m was obtained as 58.0 ± 0.4 °C for all of the oligomers studied, although shoulder peaks at lower temperatures were observed during trimeric and tetrameric cyt *c* dissociations. These shoulder peaks indicate that larger oligomers become easier to dissociate, and smaller oligomers as well as monomeric cyt *c* are more stable under nondenaturing conditions. In the presence of 30% PEG 200 and 200 mM $(NH_4)_2HPO_4$, the ΔH for dimer-to-monomer and trimer-to-monomer dissociations were -12 ± 3 and -23 ± 3 kcal/mol, suggesting stabilization of the dimer and trimer by closed-ended domain swapping and cyclization, respectively.

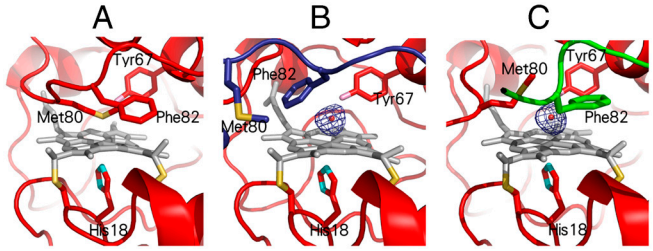

Fig. 2. Active site structures of oxidized monomeric and oligomeric cyt *c*. (*A*) Structure of monomeric cyt *c* reported previously (PDB ID code 1HRC). (*B*) Structure of dimeric cyt *c* solved in this study. (*C*) Structure of trimeric cyt *c* solved in this study. The blue strand in the dimeric structure and green strand in the trimeric structure are regions from other molecules. The atoms (probably oxygen species) that are coordinated to the heme irons in dimeric and trimeric cyt *c* are currently assigned as hydroxide ions and are depicted as small balls. *Fo-Fc* omit electron density maps contoured at 3σ for the hydroxide ion coordinated to heme iron (*B* and *C*) are shown as a blue mesh.

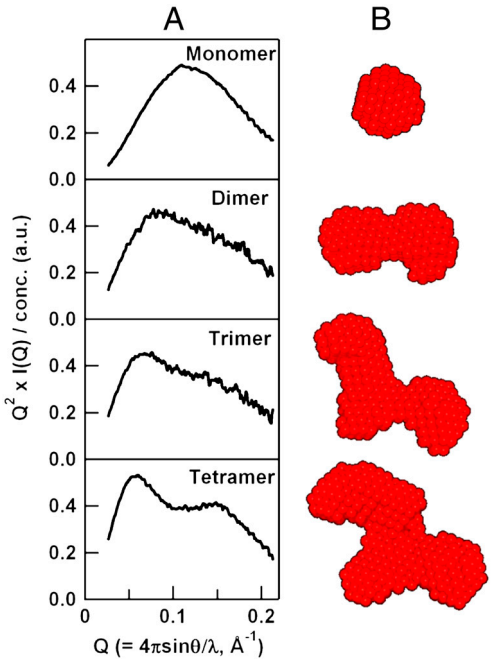

Fig. 3. Structures of oxidized monomeric and oligomeric cyt *c* in solution estimated by small-angle X-ray scattering curves. (*A*) Small-angle X-ray scattering curves of monomeric and oligomeric cyt *c* shown by Kratky plots. (*B*) Surface envelopes of monomeric and oligomeric cyt *c* obtained from the scattering curves.

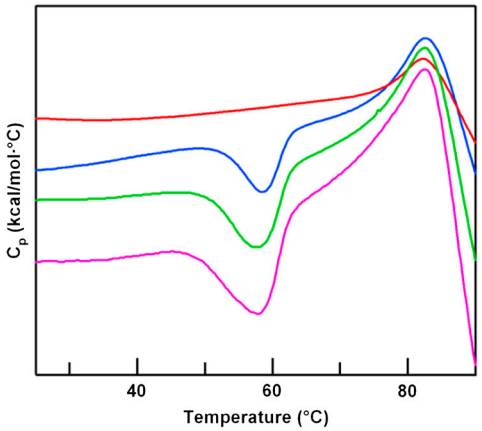

Fig. 4. Differential scanning calorimetry thermograms of oxidized, monomeric, and oligomeric cyt *c*. Thermograms of monomeric (red), dimeric (blue), trimeric (green), and tetrameric cyt *c* (pink). Measurement conditions: sample concentration: 100 μM (heme); buffer: 50 mM potassium phosphate buffer; pH: 7.0.

Discussion

Many domain-swapped structures of proteins have been revealed (12, 23, 24). Domain swapping of a single α-helix has also been reported in the dimeric structures of RNase A (N terminus) and staphylococcal nuclease (25, 26). Similarly, the same single C-terminal helix was swapped in both dimeric and trimeric cyt *c*. The domain-swapped dimeric structure of serpin was recently solved, and successive domain swapping of a single domain for polymerization has been suggested from the dimeric structure (14). For higher-order oligomers, domain swapping in RNase A has been suggested but N and C domains both swap and form various oligomers (27). However, successive domain swapping has been suggested as a mechanism for forming fibrils of RNase A (3D domain-swapped zipper-spine model) (12, 28). Barnase and an antibody fragment have been reported to form trimeric structures by domain swapping, but their oligomerization processes have not been elucidated (29, 30).

Both dimeric and trimeric cyt *c* exhibited closed-ended domain-swapped structures in crystals. The SAXS measurements demonstrated an equilibrium between the open-ended linear and closed-ended cyclic forms for trimeric cyt *c* in solution, where the equilibrium was shifted toward the cyclic form by addition of PEG and $(NH_4)_2HPO_4$. A linear structure was also observed for tetrameric cyt *c* by SAXS measurements. Because the absorption and CD spectra of cyt *c* oligomers with sizes of 30–50 mers were similar to those of the dimer and trimer, large and small oligomers may possess similar protein conformations. These results strongly suggest a successive domain-swapping mechanism in cyt *c* polymerization (Fig. 5). Native cyt *c* forms a stable monomeric globular structure (Fig. 5*A*). By perturbation such as addition of ethanol, cyt *c* may convert to a C-terminal open-ended form (Fig. 5*B*), and the corresponding C-terminal region of another cyt *c* molecule may occupy the vacant area, thus producing a dimer (Fig. 5*C*). In the dimeric form, the C-terminal region of either one of the cyt *c* molecules may not occupy the vacant area of the other protein (Fig. 5*C*). However, the C-terminal open-ended dimer may convert to a closed-ended domain-swapped structure in the presence of PEG and $(NH_4)_2HPO_4$ (Fig. 5*D*) (Figs. S3 and S4). For the C-terminal open-ended dimer, the C-terminal region of another cyt *c* molecule may occupy the vacant area and produce a linear trimer (Fig. 5*E*). Similar to the dimer, the linear trimer may convert to a cyclic trimer by addition of PEG and $(NH_4)_2HPO_4$ (Fig. 5*F*). The binding of the C-terminal region of one protein to the vacant area of a linear trimer may occur similarly forming a tetramer (Fig. 5*G*), and the successive domain swapping may occur continuously, eventually forming a protein polymer.

Dissociation of Met80 from the heme iron and coordination of a hydroxide ion were observed in the crystal structures of dimeric and trimeric cyt *c*. It has been reported that cyt *c* oxidizes cardiolipin by the peroxidase function resulting from cardiolipin-cyt *c* complexation during the early phase of apoptosis (6). The produced oxidized cardiolipin reduces the binding of cyt *c* to the mitochondrial inner membrane and facilitates permeabilization of the outer membrane (6). Disruption of the Met80-heme iron ligation has been shown to occur when cyt *c* binds tightly to cardiolipin in the inner mitochondrial membrane (31, 32). The present results show that cyt *c* oligomerization also leads to disruption of Met-Fe coordination, which enhances the peroxidation function of cyt *c*.

The ΔH of oligomer dissociation depended on the number of monomer units in the oligomer, where Met is recoordinated to the heme after production of monomers. The relatively small rmsd values indicate that the hydrophobic interactions between the C-terminal region and the rest of the protein are similar between monomeric and oligomeric (dimeric and trimeric) cyt *c*.

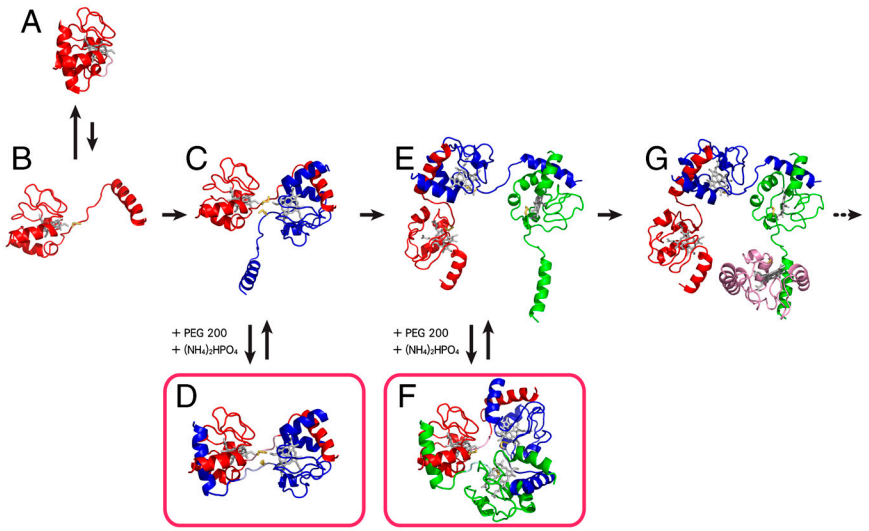

Fig. 5. Schematic summary of cyt *c* polymerization. (*A*) Crystal structure of monomeric cyt *c* (PDB ID code 1HRC). (*B*) Model of monomeric cyt *c* in solution. (*C*) Model of dimeric cyt *c* in solution. (*D*) Crystal structure of dimeric cyt *c* solved in this study. (*E*) Model of trimeric cyt *c* in solution. (*F*) Crystal structure of trimeric cyt *c* solved in this study. (*G*) Model of tetrameric cyt *c* in solution. Met80 is highlighted in yellow.

Since the ΔH of Met coordination to the heme in cyt *c* has been estimated to be −18 kcal/mol (33), the Met-Fe dissociation appears to contribute largely to the ΔH of −20 kcal/mol for oligomer dissociation. The interaction of the C terminal with the protein is not so strong, because an equilibrium seems to exist between linear and cyclic forms of trimeric cyt *c*, according to the SAXS experiments. These results support the mechanism in which cyt *c* undergoes successive domain-swapping in each extension step during oligomerization.

In conclusion, the structures of dimeric and trimeric cyt *c* suggest that cyt *c* forms oligomers successively by swapping C-terminal domains, where the Met80-heme coordination is significantly perturbed. Extension of the oligomer by one cyt *c* molecular unit would require about 20 kcal/mol. These results uncover the mechanism of cyt *c* polymerization, which could be a common protein process.

Materials and Methods

Preparation of Oligomers. Cyt *c* oligomers were prepared by dissolving about 100 mg of horse heart cyt *c* (Wako) in 10 mL of 50 mM potassium phosphate buffer, pH 7.0, followed by addition of ethanol to 60% (vol/vol). The cyt *c* solution was centrifuged and the precipitate was freeze-dried. The freeze-dried precipitate was dissolved in 10 mL of 50 mM potassium phosphate buffer, pH 7.0. After incubation of cyt *c* at 37 °C for 40 min, the cyt *c* oligomer solution was filtrated, and each oligomeric cyt *c* was purified by gel chromatography (HiLoad 26/60 Superdex 75, GE Healthcare) several times with 50 mM potassium phosphate buffer, pH 7.0. Purified cyt *c* oligomers were used immediately after purification. High order cyt *c* oligomers were purified with the Superdex 200 10/300 GL column (GE Healthcare).

Optical Absorption and CD Measurements. Absorption spectra were measured with a UV-2450 spectrophotometer (Shimadzu) using a 1-cm path-length quartz cell. CD spectra were measured with a J-725 circular dichroism spectropolarimeter (Jasco) using a 0.1-cm path-length quartz cell.

X-Ray Crystallography. Crystallization was carried out at 277 K using the sitting drop vapor diffusion method with Crystal Screening kits (Emerald Biosystems Inc.). The protein concentration was 15 mg/mL in 50 mM Tris-HCl buffer, pH 7.4. The droplets prepared by mixing 1 μL of the protein solution with 1 μL reservoir solution were equilibrated. The best reservoir solution was found to be 30% PEG 200, 200 mM $(NH_4)_2HPO_4$, and 0.1 M Tris-HCl buffer, pH 8.5.

The diffraction data were collected at the BL26B2 beam line in SPring-8. The crystal was mounted on a cryoloop and flash-frozen at 100 K in a nitrogen cryo system. The detector was MX-225 (Marreserch). The crystal to detector distance was 230 mm, and the wavelength was 0.8 Å. The oscillation angle was 0.6° and exposure time was 20 s per frame. The total number of frames was 300. The diffraction data were processed using the program *DENZO* and *SCALEPACK* (34).

The preliminary structure was obtained by a molecular replacement method (*MOLREP*) using the atomic coordinates of the monomer structure of horse cyt *c* (PDB ID code 1CRC) as a starting model. The structure refinement was performed using the program CNS (35). The molecular model was manually corrected, and water molecules were picked up in the electron density map using the program *XTALVIEW*. The data collection and refinement statistics are summarized in Table S2.

Peroxidase Activity Measurements. Peroxidase activities of monomeric and dimeric cyt *c* were measured by the oxidation of 2,2′-azino-bis(3-ethylbenzothiazoline-6-sulfonic acid) (ABTS) at 25 °C in 50 mM potassium phosphate buffer, pH 7.0. The formation of ABTS cation radical was monitored at 730 nm. The reaction mixture contained 1 μM protein (heme unit), 50 μM ABTS, and 0.2–100 mM H_2O_2.

Small-Angle X-ray Scattering. All samples were prepared in 100 mM Tris-HCl, pH 8.5. SAXS measurements were carried out using a rotating anode X-ray generator, UltraX18 (Rigaku), in which monochromatic X-ray with a wavelength of 1.54 Å was focused through a confocal Max-Flux mirror (Rigaku). Scattering profiles were collected using an X-ray image intensifier CCD detector (Hamamatsu Photonics K.K.). The sample cell with a path-length of 1 mm was controlled at 10 °C. We measured a series of oligomer dilutions, which were used to eliminate interparticle interference by extrapolation to zero protein concentration. Surface envelope models were calculated using GASBOR (36) after the treatment of the scattering profile with GNOM (37). The average structure was obtained after superimposing the independently calculated 30 models.

DSC Measurements. DSC thermograms of cyt *c* oligomers were measured at a scan rate of 1 °C/ min with VP-DSC (MicroCal, GE Healthcare) in 50 mM Tris-HCl buffer, pH 7.0, in the absence and presence of 30% PEG200 and 200 mM $(NH_4)_2HPO_4$.

ACKNOWLEDGMENTS. We thank Prof. Richard S. Margliozzo and Mr. Steven Nishida for their advice during manuscript preparation. This work was partially supported by Grants-in-Aid for Scientific Research from Ministry of Education, Culture, Sports, Science and Technology of Japan [Priority Areas, 20051016 (S.H.); Global Center of Excellence Program (Y.H.)], Japan Society for the Promotion of Science [Category B 21350095 (S.H.); 18GS0207 (Y.H.)], Japan Science and Technology Agency (S.H.), and Sankyo Foundation of Life Science (S.H.). This study was also supported by the Japanese Aerospace Exploration Agency Project (Y.H.).

1. Spierings D, et al. (2005) Connected to death: The (unexpurgated) mitochondrial pathway of apoptosis. *Science* 310:66–67.
2. Li P, et al. (1997) Cytochrome *c* and dATP-dependent formation of Apaf-1/caspase-9 complex initiates an apoptotic protease cascade. *Cell* 91:479–489.
3. Dickerson RE, et al. (1971) Ferricytochrome *c*. I. General features of the horse and bonito proteins at 2.8 Å resolution. *J Biol Chem* 246:1511–1535.
4. Banci L, et al. (1997) Solution structure of oxidized horse heart cytochrome *c*. *Biochemistry* 36:9867–9877.
5. Bushnell GW, Louie GV, Brayer GD (1990) High-resolution three-dimensional structure of horse heart cytochrome *c*. *J Mol Biol* 214:585–595.
6. Kagan VE, et al. (2005) Cytochrome *c* acts as a cardiolipin oxygenase required for release of proapoptotic factors. *Nat Chem Biol* 1:223–232.
7. de Groot NS, Ventura S (2005) Amyloid fibril formation by bovine cytochrome *c*. *Spectroscopy* 19:199–205.
8. Pertinhez TA, et al. (2001) Amyloid fibril formation by a helical cytochrome. *FEBS Lett* 495:184–186.
9. Selkoe DJ (2003) Folding proteins in fatal ways. *Nature* 426:900–904.
10. Bucciantini M, et al. (2002) Inherent toxicity of aggregates implies a common mechanism for protein misfolding diseases. *Nature* 416:507–511.
11. Kayed R, et al. (2003) Common structure of soluble amyloid oligomers implies common mechanism of pathogenesis. *Science* 300:486–489.
12. Bennett MJ, Sawaya MR, Eisenberg D (2006) Deposition diseases and 3D domain swapping. *Structure* 14:811–824.
13. Chiti F, Dobson CM (2009) Amyloid formation by globular proteins under native conditions. *Nat Chem Biol* 5:15–22.
14. Yamasaki M, Li W, Johnson DJ, Huntington JA (2008) Crystal structure of a stable dimer reveals the molecular basis of serpin polymerization. *Nature* 455:1255–1258.
15. Margoliash E, Lustgarten J (1962) Interconversion of horse heart cytochrome *c* monomer and polymers. *J Biol Chem* 237:3397–3405.
16. Crestfield AM, Stein WH, Moore S (1962) On the aggregation of bovine pancreatic ribonuclease. *Arch Biochem Biophys* Suppl 1:217–222.
17. Schejter A, Glauser SC, George P, Margoliash E (1963) Spectra of cytochrome *c* monomer and polymers. *Biochim Biophys Acta* 73:641–643.
18. Lu Y, Casimiro DR, Bren KL, Richards JH, Gray HB (1993) Structurally engineered cytochromes with unusual ligand-binding properties: expression of *Saccharomyces cerevisiae* Met-80 → Ala iso-1-cytochrome *c*. *Proc Natl Acad Sci USA* 90:11456–11459.
19. Silkstone GG, Cooper CE, Svistunenko D, Wilson MT (2005) EPR and optical spectroscopic studies of Met80X mutants of yeast ferricytochrome *c*. Models for intermediates in the alkaline transition. *J Am Chem Soc* 127:92–99.
20. Shiraki K, Nishikawa K, Goto Y (1995) Trifluoroethanol-induced stabilization of the alpha-helical structure of beta-lactoglobulin: Implication for non-hierarchical protein folding. *J Mol Biol* 245:180–194.
21. Ying T, et al. (2009) Tyrosine-67 in cytochrome *c* is a possible apoptotic trigger controlled by hydrogen bonds *via* a conformational transition. *Chem Commun* 4512–4514.
22. Belikova NA, et al. (2006) Peroxidase activity and structural transitions of cytochrome *c* bound to cardiolipin-containing membranes. *Biochemistry* 45:4998–5009.
23. Newcomer ME (2002) Protein folding and three-dimensional domain swapping: A strained relationship? *Curr Opin Struc Biol* 12:48–53.
24. Rousseau F, Schymkowitz JW, Itzhaki LS (2003) The unfolding story of three-dimensional domain swapping. *Structure* 11:243–251.
25. Liu Y, Hart PJ, Schlunegger MP, Eisenberg D (1998) The crystal structure of a 3D domain-swapped dimer of RNase A at a 2.1- Å resolution. *Proc Natl Acad Sci USA* 95:3437–3442.
26. Green SM, Gittis AG, Meeker AK, Lattman EE (1995) One-step evolution of a dimer from a monomeric protein. *Nat Struct Biol* 2:746–751.
27. Liu Y, Gotte G, Libonati M, Eisenberg D (2002) Structures of the two 3D domain-swapped RNase A trimers. *Protein Sci* 11:371–380.
28. Sambashivan S, Liu Y, Sawaya MR, Gingery M, Eisenberg D (2005) Amyloid-like fibrils of ribonuclease A with three-dimensional domain-swapped and native-like structure. *Nature* 437:266–269.

29. Zegers I, Deswarte J, Wyns L (1999) Trimeric domain-swapped barnase. *Proc Natl Acad Sci USA* 96:818–822.
30. Pei XY, Holliger P, Murzin AG, Williams RL (1997) The 2.0-Å resolution crystal structure of a trimeric antibody fragment with noncognate VH-VL domain pairs shows a rearrangement of VH CDR. *Proc Natl Acad Sci USA* 94:9637–9642.
31. Bernad S, et al. (2004) Interaction of horse heart and *Thermus thermophilus* type *c* cytochromes with phospholipid vesicles and hydrophobic surfaces. *Biophys J* 86:3863–3872.
32. Tuominen EK, Wallace CJ, Kinnunen PK (2002) Phospholipid-cytochrome *c* interaction: Evidence for the extended lipid anchorage. *J Biol Chem* 277:8822–8826.
33. George P, Glauser SC, Schejter A (1967) The reactivity of ferricytochrome *c* with ionic ligands. *J Biol Chem* 242:1690–1695.
34. Otwinowski Z, Minor W (1997) Processing of X-ray diffraction data collected in oscillation mode. *Methods Enzymol* 276:307–326.
35. Brünger AT, et al. (1998) Crystallography & NMR system: A new software suite for macromolecular structure determination. *Acta Crystallogr D* 54:905–921.
36. Svergun DI (1992) Determination of the regularization parameter in indirect-transform methods using perceptual criteria. *J Appl Crystallogr* 25:495–503.
37. Svergun DI, Petoukhov MV, Koch MHJ (2001) Determination of domain structure of proteins from X-ray solution scattering. *Biophys J* 80:2946–2953.